XI International Conference on Computational Plasticity. Fundamentals and Applications
COMPLAS XI
E. Oñate, D.R.J. Owen, D. Peric and B. Suárez (Eds)

SIMULATION OF DP-STEELS BASED ON STATISTICALLY SIMILAR REPRESENTATIVE VOLUME ELEMENTS AND 3D EBSD DATA

D. BRANDS*, D. BALZANI*, J. SCHRÖDER* AND D. RAABE†

*Institute of Mechanics, Faculty of Engineering, Department of Civil Engineering,
University of Duisburg-Essen,
Universitätsstraße 15, 45141 Essen, Germany
e-mail: dominik.brands@uni-due.de

† Max-Planck-Institut für Eisenforschung GmbH
Dept. Microstructure Physics and Metal Forming
Max-Planck-Straße 1, 40237 Düsseldorf, Germany

Key words: multiscale problems, homogenization, material properties, finite plasticity, microstructures, statistically similar RVE, EBSD

Abstract. Micrographs of a dual-phase steel obtained from a EBSD-FIB imaging are analyzed with respect to a set of statistical measures. Then the applicability of this data to the construction of statistically similar representative volume elements (SSRVEs) is discussed. These SSRVEs are obtained by minimizing a least-square functional taking into account differences of statistical measures computed for a given reference microstructure and the SSRVE, cf. [11]. For an analysis of the mechanical response the FE^2-method is used and a series of virtual experiments shows the accordance of the response of the SSRVE to the one of the reference microstructure. In order to demonstrate the performance of the proposed procedure some representative numerical examples are given.

1 Introduction

To achieve the demands for high strength and good formability modern steels as e.g. dual-phase steels make use of multi-phase microstructures, see e.g. [4], [5]. Since the micromechanics of these micro-heterogeneous materials mainly govern the overall material behavior they need to be taken into account when computer simulations of deep-drawing processes are performed. For this purpose the FE^2-method provides a suitable numerical tool, see e.g. [12], [7], [10]. There a microscopic boundary value problem, which is based on the definition of a representative volume element (RVE), is solved at each macroscopic integration point. However, this method is computationally expensive if substructures of real micrographs are used as an RVE since these are typically too complex for efficient

discretizations at the microscale. For that reason the estimation of a suitable RVE is a challenging task. Thus, we analyze in a first step several micrographs obtained from a 3D EBSD imaging. Afterwards we construct statistically similar RVEs (SSRVEs) which are characterized by a strongly reduced complexity than usual RVEs and which therefore lead to procedures of significantly improved efficiency.
The paper is organized as follows. In the first section we introduce several statistical measures for the characterization of microstructural morphology and afterwards analyze them for micrographs from a three-dimensional EBSD-FIB imaging. Section 3 describes the construction method of SSRVEs and the application to a dual-phase steel microstructure. This paper is closed with numerical examples and a conclusion.

2 Characterization of the Morphology

In this section we are interested in the analysis of the morphology of dual-phase steels, which are characterized by a martensitic inclusion phase embedded in a ferritic matrix phase. In addition to the individual mechanical properties of both constituents, the macroscopic mechanical behavior is also significantly governed by the morphology of the inclusion phase at the microscale. Therefore we introduce in the following subsections several statistical measures characterizing the inclusion morphology and analyze a stack of two-dimensional micrographs obtained from a 3D EBSD-FIB imaging with respect to these measures.

2.1 Statistical Measures

A well-known fundamental measure for the characterization of the morphology is the volume fraction, also referred to as phase fraction. This measure is defined for the inclusion phase i by

$$\mathcal{P}_V^{(i)} := \frac{V_{(i)}}{V} \ , \tag{1}$$

where $V_{(i)}$ denotes the volume of the phase i. In [8] additional basic parameters for the description are given, e. g. surface density and integrals of curvature. Since typically also direction-dependend information regarding e.g. laminate-like arranged inclusions leading to a macroscopically anisotropic behavior, these measures are not sufficient for the characterization of complex microstructures, see [2]. Thus, we consider statistical measures of higher order to capture microscopic information regarding periodic and directional characteristics in the microstructure.
As a first measure of higher order we consider the (discrete) spectral density (SD) for the inclusion phase computed from the binary image of the micrograph. The SD is computed by the multiplication of the (discrete) Fourier transform with its conjugate complex. The discrete SD is defined by

$$\mathcal{P}_{SD}(m,k) := \frac{1}{2\pi\, N_x\, N_y}\, |\mathcal{F}(m,k)|^2 \tag{2}$$

with the Fourier transform given by

$$\mathcal{F}^I(m,k) = \sum_{p=1}^{N_x}\sum_{q=1}^{N_y} \exp\left(\frac{2\,i\,\pi\,m\,p}{N_x}\right)\exp\left(\frac{2\,i\,\pi\,k\,q}{N_y}\right)\chi^I_{SD}(p,q)\,. \tag{3}$$

The maximal numbers of pixels in the considered binary image are given by N_x and N_y; the indicator function is defined as

$$\chi_{SD} := \begin{cases} 1, & \text{if } (p,q) \text{ is in the inclusion phase} \\ 0, & \text{else}\,. \end{cases} \tag{4}$$

A further statistical measure is provided by the lineal-path function, which describes the probability that a complete line segment $\overrightarrow{\boldsymbol{x_1 x_2}}$ is located in the same phase, see [13]. For its mathematical description we consider the modified indicator function

$$\chi_{LP}(\overrightarrow{\boldsymbol{x}_1\boldsymbol{x}_2}) := \begin{cases} 1, & \text{if} \quad \overrightarrow{\boldsymbol{x}_1\boldsymbol{x}_2} \quad \text{is in the inclusion phase} \\ 0, & \text{else}\,. \end{cases} \tag{5}$$

For two-dimensional binary images of statistically homogeneous and ergodic inclusion-matrix microstructures the lineal-path function is computed by

$$\mathcal{P}^I_{LP}(m,k) = \frac{1}{N_x N_y}\sum_{p=1}^{N_x}\sum_{q=1}^{N_y}\chi^I_{LP}(\overline{\boldsymbol{x}_m\boldsymbol{x}_k})\,, \tag{6}$$

for a periodic unitcell. Herein, $N_x \times N_y$ defines the number of pixels of the binary microstructure image to be analyzed. Efficient procedures for the calculation of the lineal-path function can be obtained by defining suitable templates, cf. [15].

2.2 Analysis of Ensemble Average

In this section we analyze several micrographs with respect to the statistical measures introduced in the previous subsection. They are obtained from a metallographic characterization using the 3D electron backscatter diffraction (3D EBSD) method. Thereby a joint high-resolution field emission SEM/EBSD set-up is coupled with a focused ion beam system (FIB) and provides a set of cross-sectional planes of the considered dual-phase steel. The equipment and the geometric arrangement is shown in Fig. 1a,b

The sample of the considered dual-phase steel is mounted on a tiltable holder inside the equipment, cf. Fig. 1b. During the investigation the sample is tilt between two positions: the cutting and the EBSD position. In the cutting position the FIB system milling thin layers (10 nm - 1 μm thick) from the investigated surface of the sample. The other position is used for the EBSD analysis, where an electron beam is focussed onto the milled surface and the back scatter diffraction patterns are monitored by the EBSD camera. Due to different diffraction patterns several properties of the sample can be analyzed, e. g. crystal orientations and grain size. Additionally a reconstruction of the in-plane morphology

a) b) c)

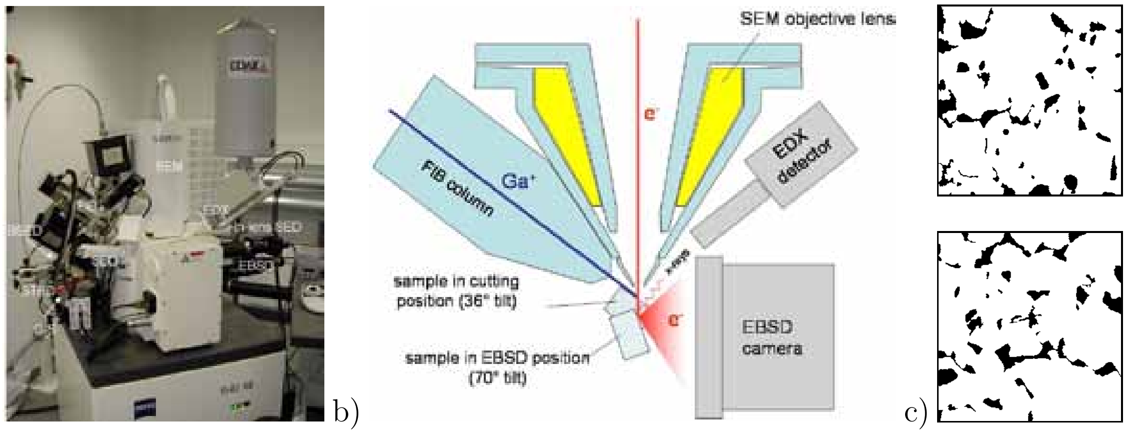

Figure 1: 3D EBSD: a) equipment, b) technical setup, cf. [6], and c) two examples of obtained cross-sections of the considered dual-phase. The micrographs are color-coded with respect to the phases (white: ferrite, black: martensite) and with an approximate dimension of $15 \times 15\,\mu\mathrm{m}^2$.

of the ferritic matrix and the martensitic inclusion phase are possible based on this back scatter diffraction patterns. Such micrographs are exemplarily depicted in Fig. 1c. For more details concerning the 3D EBSD method we refer to [6, 3, 14].
In this contribution we use a set of 50 micrographs obtained by the aforementioned technique. The volume fraction, the spectral density and the lineal-path function of all slices are calculated from the binary images. Considering a constant distribution density for the individual samples (micrographs) the ensemble average $\overline{\mathcal{P}_{SM}}$ of the particular statistical measures $\mathcal{P}_{SM}$ can be computed by

$$\overline{\mathcal{P}_{SM}} = \frac{1}{n_\alpha} \sum_{\alpha=1}^{n_\alpha} \mathcal{P}_{SM} \quad \text{with } n_\alpha \text{ samples}\,, \tag{7}$$

where n_α denotes the number of samples. The relative standard deviation is given by

$$\hat{S}_{SM} = S_{SM} \Big/ \overline{\mathcal{P}_{SM}} \quad \text{with} \quad S_{SM} = \sqrt{\frac{\sum_{n=1}^{n_\alpha} (\mathcal{P}_{SM}(\alpha) - \overline{\mathcal{P}_{SM}})}{n_\alpha(n_\alpha - 1)}}\;, \tag{8}$$

where S_{SM} denotes the absolute standard deviation and $\mathcal{P}_{SM}(\alpha)$ the individual value of the statistical measure computed from the sample α. Note, that due to the two-dimensional character of the spectral density and lineal-path function we apply the latter equations to each point in the image space. The results are represented by two-dimensional arrays $\hat{S}_{SM}(p,q)$ with the dimension $N_x^{SM} \times N_y^{SM}$. To achieve a scalar-valued comparative measure we introduce the mean relative standard deviation

$$\hat{S}_{SM}^{\varnothing} = \sqrt{\frac{1}{N_X N_y} \sum_{p=1}^{N_X^{SM}} \sum_{q=1}^{N_y^{SM}} \left[\hat{S}_{SM}(p,q)\right]^2}\;. \tag{9}$$

Finally, we obtain the values of the relative standard deviation and the mean relative standard deviations

$$\hat{S}_V = 0.45 \cdot 10^{-1}\,, \quad \hat{S}^{\varnothing}_{SD} = 1.57 \cdot 10^{-1}\,, \quad \text{and} \quad \hat{S}^{\varnothing}_{LP} = 2.36 \cdot 10^{-1} \tag{10}$$

of the volume fraction (V), spectral density (SD) and the lineal-path function (LP), respectively. From the relatively low values we conclude, that the distribution of the considered statistical measures along the thickness direction is relatively homogeneous. This leads to the conclusion that two-dimensional micrograph data might be suffient for the construction of two-dimensional SSRVEs, which in turn may enter numerical calculations of two-dimensional boundary value problems. Thus, in the following section we use one micrograph taking into account a larger region as the reference microstructure for the construction of the SSRVEs, cf. Fig. 2a.

3 Statistically Similar RVEs

The choice of the representative volume elements (RVE) is an essential task in the context of direct micro-macro approaches. In general, the RVE is determined by the smallest possible sub-domain reflecting the macroscopic behavior of the target material in an adequate manner. However, these RVEs are typically too complex for efficient calculations. Therefore, the construction of statistically similar RVEs (SSRVEs) which are characterized by a significantly lower complexity are to be constructed in this section, cf. [1], where the method is introduced taking into account the volume fraction and the spectral density. The main effort of such SSRVEs is that due to the reduced complexity a significantly reduced number of finite elements is required for the discretization of the microscopic boundary value problem in the context of FE^2-calculations. As a result, a decreased computational cost is obtained.

3.1 Method for Construction

The main idea for the construction of SSRVEs is to minimize a least-square functional taking into account differences of statistical measures computed for the real target microstructure and the SSRVE. Thereby, it is assumed that the inclusion phase morphology mainly influences the overall behavior provided that the material properties of the individual phases are known. The minimization problem is formulated by

$$\mathcal{L}(\boldsymbol{\gamma}) = \sum_{L=1}^{n_{sm}} \omega_i \, \mathcal{L}^{(L)}_{SM}(\boldsymbol{\gamma}) \quad \rightarrow \quad \min\,, \tag{11}$$

where the individual least-square functionals $\mathcal{L}^{(L)}_{SM}$ are based on the difference of suitable statistical measures. The weighting factor ω levels the influence of the individual measures. The vector $\boldsymbol{\gamma}$ describes the parameterization of the inclusion phase morphology. Here, splines are used for the parameterization and thus, the sampling point coordinates enter the generalized vector $\boldsymbol{\gamma}$ of the degrees of freedom of the minimization problem given in (11). In this contribution five different types of SSRVEs are considered: Type I taking into account one inclusion with three sampling points (leading to an inclusion with a convex shape), Type II with one inclusion and four sampling points, Type III with two inclusions and three sampling points each, Type IV with two inclusions and four sampling points each and Type V with three inclusions and three sampling points each. Due to the discrete character of the statistical measures used in the minimization problem (11) the energy surface is not smooth and therefore, no gradient-based optimization method can be applied. Therefore, the moving-frame algorithm proposed in [2] is used. In [11] we showed that the combination of the volume fraction (V), the spectral density (SD) and the lineal-path function (LP) as statistical measures leads to promising results in the context of two-phase materials, whose macroscopic mechanical response is mainly governed by the microstructural morpohology. From this we define the three individual least-square functionals

$$\begin{aligned}
\mathcal{L}_V(\boldsymbol{\gamma}) &:= \left(1 - \tfrac{\mathcal{P}_V^{SSRVE}(\boldsymbol{\gamma})}{\mathcal{P}_V^{real}}\right)^2 , \\
\mathcal{L}_{SD}(\boldsymbol{\gamma}) &:= \frac{1}{N_x\, N_y} \sum_{m=1}^{N_x} \sum_{k=1}^{N_y} \left(\mathcal{P}_{SD}^{real}(m,k) - \mathcal{P}_{SD}^{SSRVE}(m,k,\boldsymbol{\gamma})\right)^2 , \qquad (12) \\
\mathcal{L}_{LP}(\boldsymbol{\gamma}) &:= \frac{1}{N_x\, N_y} \sum_{m=1}^{N_x} \sum_{k=1}^{N_y} \left(\mathcal{P}_{LP}^{real}(m,k) - \mathcal{P}_{LP}^{SSRVE}(m,k,\boldsymbol{\gamma})\right)^2 .
\end{aligned}$$

It is remarked that for the computation of the statistical measures $\mathcal{P}_{SD}$ and $\mathcal{P}_{LP}$ periodic expansions of the SSRVE are considered by placing as much SSRVEs as needed at each other periodically. Following equation (11) we end up with the objetive function

$$\mathcal{L}(\boldsymbol{\gamma}) = \omega_V \mathcal{L}_V(\boldsymbol{\gamma}) + \omega_{SD} \mathcal{L}_{SD}(\boldsymbol{\gamma}) + \omega_{LP} \mathcal{L}_{LP}(\boldsymbol{\gamma}) , \qquad (13)$$

which is minimized using the aforementioned optimization algorithm.

3.2 Two-Dimensional SSRVEs

Now we apply the method for the construction of SSRVEs to a real dual-phase steel microstructure and consider the micrograph shown in Fig. 2 as target structure. Considering the objective function (13) and the five different types of inclusion parameterization we receive from minimizing (11) five realizations of SSRVEs. The finite element discretization of these SSRVEs required for the following mechanical error analysis are shown in Fig. 3. After the SSRVE construction we have to analyze the capability of the resulting structures to represent the macroscopic mechanical response of the target structure. Thus, we consider three different simple macroscopic virtual experiments: horizontal tension, vertical tension and simple shear. FE^2-simulations taking into account the target structure at the microscale are compared with FE^2-calculations focussing on the constructed SSRVEs.

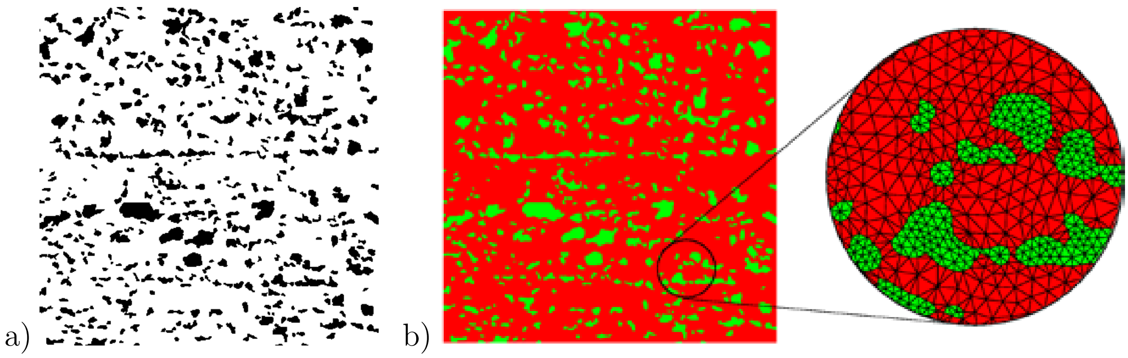

Figure 2: Target Structure: a) real micrograph with a dimension of approximately $100 \times 100\,\mu\text{m}^2$ and b) discretization by 6-noded triangular finite elements resulting in approximately 150,000 degrees of freedom.

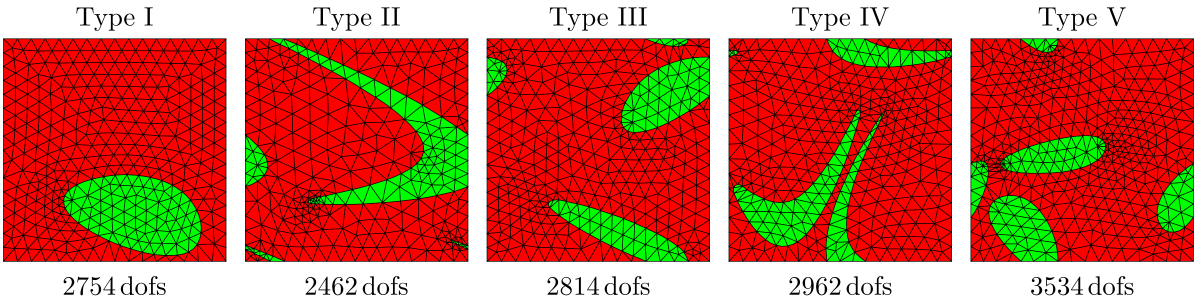

Figure 3: Discretization of the resulting SSRVEs with the associated number of degrees of freedom (dofs).

For this purpose microscopic boundary value problems where a discretization by triangular Finite Elements with quadratic ansatz functions for the displacements are considered. Furthermore, plain stress conditions and periodic boundary conditions are applied. The individual constituents at the microscale are modeled by a standard J_2-finite plasticity model, for details see e. g. [9]. An exponential von Mises hardening law is used, i.e.

$$\beta = y_\infty + (y_0 - y_\infty)\exp(-\eta\alpha) + h\,\alpha\,, \tag{14}$$

with $\beta = \partial_\alpha \psi^p$ and ψ^p denoting the strain energy function associated to the hardening; α are the equivalent plastic strains. The material parameters are adjusted to experiments performed on purely ferritic and purely martensitic test specimens and given in Table 1.

Table 1: Material parameters of the single phases

phase	λ [MPa]	μ [MPa]	y_0 [MPa]	y_∞ [MPa]	η [-]	h [-]
matrix	118,846.2	79,230.77	260.0	580.0	9.0	70.0
inclusion	118,846.2	79,230.77	1000.0	2750.0	35.0	10.0

Table 2: Values of the objective functions $\mathcal{L}$ and the mechanical errors $\widetilde{r}$. n_{ele} denotes the number of finite elements in the discretization.

SSRVE	$\mathcal{L}$ $[10^{-3}]$	$\mathcal{L}_V$ $[10^{-5}]$	$\mathcal{L}_{SD}$ $[10^{-4}]$	$\mathcal{L}_{LP}$ $[10^{-5}]$	n_{ele}	$\widetilde{r}_x$ [%]	$\widetilde{r}_y$ [%]	$\widetilde{r}_{xy}$ [%]	$\widetilde{r}$ [%]
I	39.41	238.05	230.96	139.38	656	1.16 ± 0.29	1.58 ± 0.39	3.34 ± 0.91	2.24
III	8.66	8.82	62.87	22.81	670	0.26 ± 0.20	2.24 ± 0.52	0.41 ± 0.22	1.32
V	4.22	1.42	36.62	5.41	850	1.12 ± 0.35	0.92 ± 0.26	1.10 ± 0.23	1.05
II	9.29	14.90	71.31	20.08	582	8.24 ± 2.10	2.10 ± 0.31	7.45 ± 2.87	6.53
IV	3.70	4.33	33.88	2.73	708	2.22 ± 0.80	4.89 ± 1.24	2.43 ± 1.22	3.40

As comparative mechanical measures we consider the relative errors r_x, r_y and r_{xy} defined as the deviation of the resulting macroscopic SSRVE stress response from the target structure response at each evaluation point i for the three virtual experiments:

$$r_x^{(i)} = \frac{\overline{\sigma}_{x,i}^{\text{real}} - \overline{\sigma}_{x,i}^{\text{SSRVE}}}{\overline{\sigma}_{x,i}^{\text{real}}}, \qquad r_y^{(i)} = \frac{\overline{\sigma}_{y,i}^{\text{real}} - \overline{\sigma}_{y,i}^{\text{SSRVE}}}{\overline{\sigma}_{y,i}^{\text{real}}}, \qquad r_{xy}^{(i)} = \frac{\overline{\sigma}_{xy,i}^{\text{real}} - \overline{\sigma}_{xy,i}^{\text{SSRVE}}}{\overline{\sigma}_{xy,i}^{\text{real}}}, \tag{15}$$

where only values with non-vanishing denominators are taken into account. In addition to that, the average errors for each experiment

$$\widetilde{r}_{x,y,xy} = \sqrt{\frac{1}{n_{ep}} \sum_{i=1}^{n_{ep}} [r_{x,y,xy}^{(i)}]^2} \quad \text{with} \quad r_{x,y,xy}^{(i)} := r\left(\tfrac{i}{n} \triangle l_{\max}/l_0\right) \tag{16}$$

and the overall comparative measure

$$\widetilde{r}_{\varnothing} = \sqrt{\frac{1}{3}\left(\widetilde{r}_x^2 + \widetilde{r}_y^2 + \widetilde{r}_{xy}^2\right)} \tag{17}$$

are taken into account for quantitative statements with respect to the performance of the individual SSRVEs. The total number of evaluation points i is denoted by n_{ep}. The mechanical response of the five SSRVEs in the three virtual experiments are calculated using the FE^2-scheme. The results of the construction of the SSRVEs are summarized in Tab. 2. Therein we order the results of the SSRVE types seperately with respect to the number of sampling points. First, it can be observed that with increasing complexity, i.e. higher numbers of inclusions, the value of the objective function $\mathcal{L}$ decreases. Second, it turns out that Type V is showing satisfying results in all virtual experiments and has consequently the lowest value of the overall error $\widetilde{r}$. Thus, we consider Type V as the "best" SSRVE in this analysis and use it in a numerical example in the next chapter.

4 Numerical Example

Now we consider a macroscopically inhomogeneous FE^2-simulation to show the capability of the SSRVE. Therefore, we consider a radially loaded circular disk with a hole,

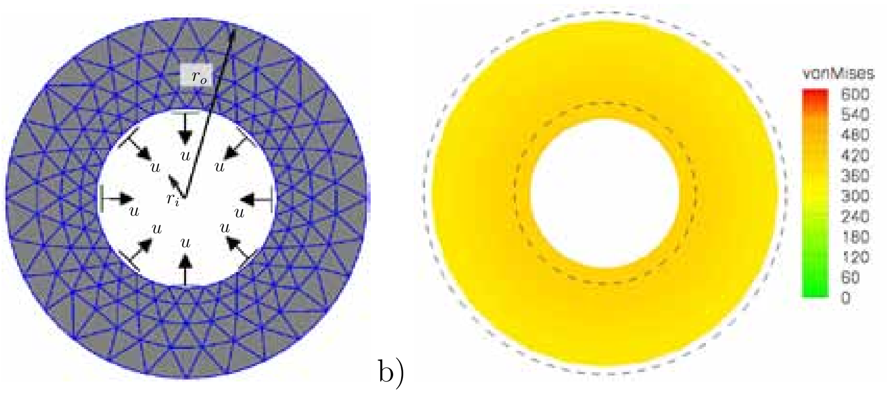

a) b)

Figure 4: Radially loaded circular disk: a)Macroscopic boundary value problem, b)von Mises stress distribution of the computation using a phenomenological material law (finite J_2 plasticity) at the macroscale.

discretized by 252 triangular elements with quadratic ansatz functions and plain strain conditions. The outer radius of the disk is $r_o = 4\,\mathrm{cm}$ and the inner one is $r_i = 2\,\mathrm{cm}$, see Fig. 4a. The load is applied on the inner radius of the disk and pulls the inner border radially inwards up to a displacement of $u = 0.35\,\mathrm{cm}$. This boundary value problem is known to be an approximation for a deep-drawing process of a cup if the outer part of the plate is to be analyzed.

Firstly, we use a phenomenological material law to describe the mechanical behavior in each macroscopic integration point and consequently it represents a purely macroscopic computation. We apply the same finite J_2 plasticity model as for the individual phases of the microstructures. The material parameters are adjusted such that the mechanical behavior matches the response of the target structure in the three virtual experiments as similarly as possible. Here we already observe that only the tensions tests can be represented accurately in contrast to the simple shear test. In Fig. 4b the results of the purely macroscopic computation of the circular disk are shown. A slightly graded stress distribution with a range about 350 MPa at the outer radius to 430 MPa at the inner one is observed. These results are now compared with the FE^{2}simulation using the SSRVE Type V at the microscale, which shows the "best" accuracy regarding the mechanical behavior of the real microstructure in the aforementioned virtual experiments. In Fig. 5 the results of this FE^2-simulation are depicted, where we show the macroscopic response top left. For the analysis of the microscopic results we select three integration points at the macroscale and place the associated microstructures also in Fig. 5, where contour plots of the von Mises stresses are shown. At the macroscale the stress ranges from about 400 MPa at the outer radius to 630 MPa at the inner one. The maximum stress level at the microscale is significantly higher as at the macroscale, up to a factor of two. Compared to the purely macroscopic simulation this is a higher maximum stress and has a stronger gradient in radial direction. These aspects show the advantages of a FE^{2}simulation because it offers a more critical view on the stress levels at the macro- and microscale and consequently provides information which might be important for failure initialization analysis.

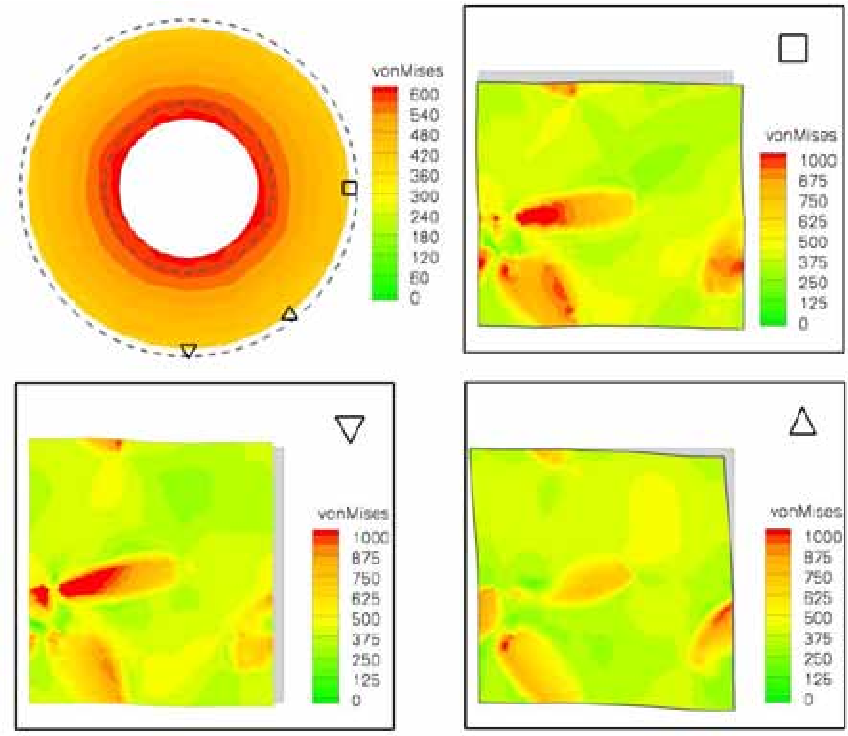

Figure 5: Results of the FE^2-simulations based on SSRVE Type V with the von Mises stress distributions in the deformed microstructures for three selected positions. The symboles in the upper right corner of the images for the microscopic response represent the link to the macroscopic position; the grey area behind the microstructure indicates the undeformed configuration.

5 Conclusions

A stack of micrographs of a dual-phase steel, which was obtained from a 3D EBSD imaging, was analyzed with respect to the distribution of three statistical measures: the volume fraction, the spectral density and the lineal-path function. From this it was observed that the measures show a relatively low variance along the thickness direction. Thus, based on these results only one micrograph was considered for the construction of statistically similar RVEs. Then, it was shown in several virtual experiments that the constructed SSRVEs are able to represent the mechanical behavior of the real microstructure, while the number of degrees of freedom is significantly decreased. By comparing the mechanical response observed in three different virtual experiments of different types of SSRVEs with the mechanical behavior of the target microstructure a number of three convex inclusions (Type V) turned out to be sufficient for the representation of the original microstructure. As an example this SSRVE was used in a macroscopically inhomogeneous boundary value problem and compared with the response obtained from a purely macroscopic computation.

Acknowledgement: The financial support of the "Deutsche Forschungsgemeinschaft" (DFG), research group MICROPLAST (FG 797) on "Analysis and Computation of Microstructures in Finite Plasticity", projects TP7 "High resolution scanning electron back scatter diffaction experiments of local crystallographic orientation patterning during plastic deformation" and TP8 "Statistically similar representative microstructures in elasto-plasticity" (SCHR 570/8-2) is gratefully acknowledged.

REFERENCES

[1] D. Balzani, J. Schröder, and D. Brands, FE^2-Simulation of Microheterogeneous Steels based on Statistically Similar RVE's, *IUTAM Bookseries, 1, Vol. 21, IUTAM Symposium on Variational Concepts with applications to the mechanics of materials, Bochum, September 22-26, 2008*, 15–28, 2010.

[2] D. Balzani, D. Brands, J. Schröder, and C. Carstensen, Sensitivity Analysis of Statistical Measures for the Reconstruction of Microstructures Based on the Minimization of Generalized Least-Square Functionals, *Technische Mechanik*, **30**, 297–315, 2010.

[3] A. Bastos, S. Zaefferer, D. Raabe, C. Schuh, Characterization of the Microstructure and Texture of Nanostructured Electrodeposited NiCo by use of Electron Backscatter Diffraction (EBSD), *Acta Materialia*, **54**, 2451– 2462, 2006.

[4] M. Calcagnotto, D. Ponge, D. Raabe, Orientation gradients and geometrically necessary dislocations in ultrafine grained dual-phase steels studied by 2D and 3D EBSD, *Mater. Sc. Engin. A*, **527**, 2738-2746, 2010.

[5] M. Calcagnotto, Y. Adachi, D. Ponge, D. Raabe, Deformation and fracture mechanisms in fine- and ultrafine-grained ferrite/martensite dual-phase steels and the effect of aging, *Acta Materialia*, **59**, 658-670, 2011.

[6] J. Konrad, S. Zaefferer, D. Raabe, Investigation of Orientation Gradients Around a Hard Laves Particle in a Warm Rolled Fe3Al-Based Alloy by a 3D EBSD-FIB Technique, *Acta Materialia*, **54**, 1369–1380, 2006.

[7] C. Miehe, J. Schröder, and J. Schotte, Computational homogenization analysis in finite plasticity. Simulation of texture development in polycrystalline materials, *Computer Methods in Applied Mechanics and Engineering*, **171**, 387–418, 1999.

[8] J. Ohser and F. Mücklich, *Statistical analysis of microstructures in materials science*. J Wiley & Sons, 2000.

[9] J.C. Simo, A framework for finite strain elastoplasticity based on maximum plastic dissipation and the multiplicative decomposition: Part I. Continuum formulation. *Computer Methods in Applied Mechanics and Engineering*, **66**, 199-219, 1988.

[10] J. Schröder, *Homogenisierungsmethoden der nichtlinearen Kontinuumsmechanik unter Beachtung von Stabilitätsproblemen*, Bericht aus der Forschungsreihe des Institut für Mechanik (Bauwesen), Lehrstuhl I, Habilitationsschrift, 2000.

[11] J. Schröder, D. Balzani, and D. Brands, Approximation of Random Microstructures by Periodic Statistically Similar Representative Volume Elements Based on Lineal-Path Functions, *Archive of Applied Mechanics*, DOI 10.1007/s00419-010-0462-3, 2010.

[12] R.J.M. Smit, W.A.M. Brekelmans, and H.E.H. Meijer, Prediction of the mechanical behavior of nonlinear heterogeneous systems by multi-level finite element modeling, *Computer Methods in Applied Mechanics and Engineering*, **155**, 181–192, 1998.

[13] T. Torquato, *Random heterogeneous materials. Microstructure and macroscopic properties*, Springer, 2002.

[14] S. Zaefferer, S. I. Wright, D. Raabe. Three-dimensional orientation microscopy in a focused ion beam-scanning electron microscope: A new dimension of microstructure characterization, *Metallurgica and Material Transactions A*, **39A**, 374–389, 2008.

[15] J. Zeman, *Analysis of Composite Materials with Random Microstructure*, University of Prague, Dissertation, 2003.